Synthesis and Characterization of Nb Substitution on (Bi-Pb)-2223 Superconductors

R. Asghari, L. Colakerol Arslan, H. Sedghi & H. Naghshara

Journal of Low Temperature Physics

ISSN 0022-2291
Volume 189
Combined 1-2

J Low Temp Phys (2017) 189:15-26
DOI 10.1007/s10909-017-1784-0

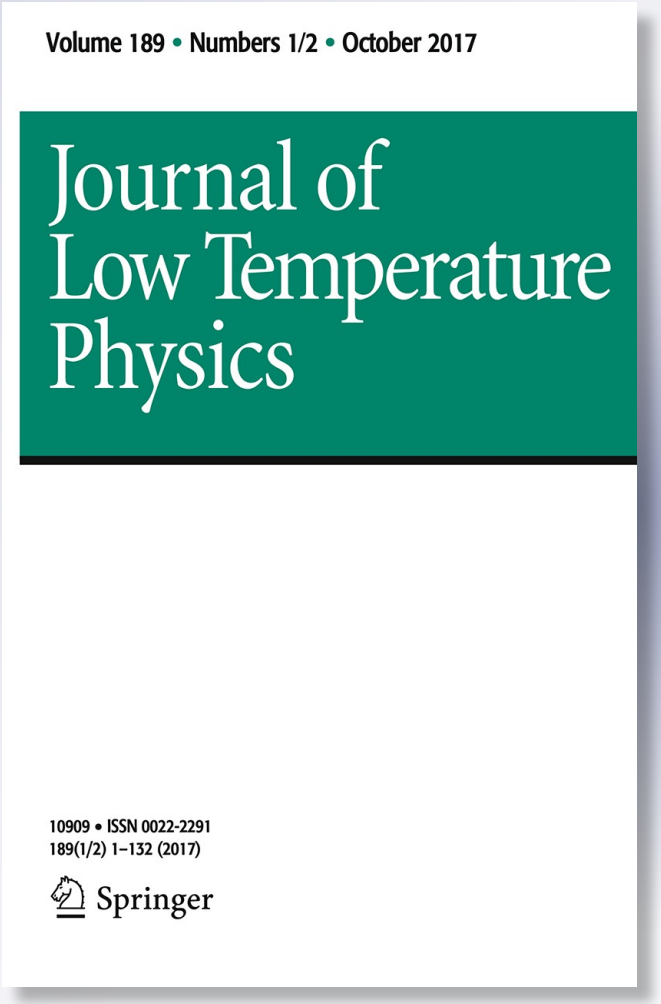

Springer

J Low Temp Phys (2017) 189:15–26
DOI 10.1007/s10909-017-1784-0

Synthesis and Characterization of Nb Substitution on (Bi-Pb)-2223 Superconductors

R. Asghari[1,3] · L. Colakerol Arslan[2] · H. Sedghi[1] · H. Naghshara[3]

Received: 16 February 2017 / Accepted: 10 June 2017 / Published online: 21 June 2017

Abstract In this study, samples of $Bi_{1.65}Pb_{0.35-x}Nb_xSr_2Ca_2Cu_3O_{10+\delta}$ were prepared by solid-state reaction method and the effect of Nb substitution for Pb on the structural and superconducting properties of this material was investigated. The room-temperature X-ray diffraction patterns indicated that all the samples have the dominant phase of high-T_c (Bi-2223). However, other phases such as Bi-2212 and some impurity phases like $SrCu_2O_2$, $CuNb_2O_6$, $CaCuO_3$ and CuO were also obtained from XRD patterns. An increasing amount of Nb^{+5} substitutions for Pb^{+2} led to a phase transition from Bi-2223 to Bi-2212. Electrical resistivity and magnetic measurements revealed that the critical temperature and the critical current density decreases with increasing Nb content due to the enhancement of Bi-2212 phase and appearance of impurities. SEM images indicated that samples porosity changes due to the disrupted grain growth with the substitution of Pb ions with Nb ions.

Keywords BSCCO high-T_c superconductors · Bi-2223 phase · XRD · SEM · Critical current density

1 Introduction

High-temperature superconductors are of interest due to both their applications in the technological promise of energy-efficient devices and the scientific challenges to

✉ R. Asghari
r.asghari@tabrizu.ac.ir

1 Department of Physics, Superconductivity Research Center, Urmia University, Urmia, Iran

2 Department of Physics, Gebze Technical University, 41400 Cayirova, Kocaeli, Turkey

3 Department of Solid State and Electronic, Faculty of Physics, Tabriz University, Tabriz, Iran

understanding the basic physical processes behind superconductivity [1,2]. After the discovery of Bi-based superconductors, great progress has been achieved in enhancing electrical, structural and superconducting properties of this type of superconductors [3]. Bi-based superconductors (BSCCO) are defined by $Bi_2Sr_2Ca_{n-1}Cu_nO_{2n+4+y}$ general formula where $n = 1, 2$ and 3 refer to the number of CuO_2 layers in the crystal structure, corresponding to the Bi-2201, 2212 and 2223 phases which have critical temperatures around 20, 85 and 110 K, respectively [4–7]. The formation of pure Bi-2223 phase is an essential issue for the synthesis of this type of superconductors. Since the formation of the 2223-phase is very slow, long periods of sintering at temperatures close to its decomposition temperature are required [8].

The critical temperature (T_c) of Bi-based copper-oxide superconductors depends on the density of mobile holes created by Cu vacancies in the CuO_2 planes [9]. There are several studies that investigate the effect of various doping elements in different sites of the BSCCO system on the hole concentration, such as rare earth elements (La, Gd, and Yb) [10,11], some alkali metals and transition elements (Hg, Ba, Y and Li) [12,13].

Coskun et al. [14] indicated that the substitution of Ca^{2+} ions by Gd^{3+} ions leads to a decrease in Cu vacancy sites. On the other hand, the replacement of Bi^{3+} ions by Pb^{2+} ions promotes Cu vacancies [15]. Therefore, substitution of Gd for Ca reduces the critical temperature and a small amount of Pb substitution for Bi increases the critical temperature. Gul et al. investigated the effect of V substitution for Bi in BSCCO system with nominal composition $Bi_{1.6-y}V_yPb_{0.4}Sr_2Ca_2Cu_3O_\delta$. They showed that with the increase in V concentration in the samples, the value of resistivity decreases, while the critical current density increases [16].

In this research, Pb^{2+} ions have been substituted by Nb^{5+} ions in order to investigate the effect of Nb on the superconducting properties of BPSCCO system. Since the ionic radius of Nb^{5+} (0.7 Å) is lower than the ionic radiuses of Bi^{3+} (0.96 Å) and Pb^{2+} (1.19 Å), there is a higher possibility of Nb occupying compared to Pb in BiO layers [17]. The melting point of niobium oxide (1512 °C) is higher compared with that of lead oxide (888 °C). Contradictory results have been reported on the effect of Nb addition on the structural and superconducting properties. It has been previously shown that addition of a slight amount of Nb_2O_5 on BSCCO improves the intergrain connectivity which results in better superconducting properties [18]. On the other band, Bilgili et al. showed that samples with Nb_2O_5 addition consisted of a mixture of Bi-2223 and Bi-2212 phases as the major constituents and non-superconducting phase Ca_2PbO_4 as the minor ones. They found that the volume fraction of high-T_c Bi-2223 phase decreased with increasing Nb addition up to $x = 0.20$. Also, they conclude that with increasing Nb addition, the surface morphology and grain connectivity of samples degraded, the grain sizes decreased, and the porosity of the samples increased [19].

In this work, the effects of Nb substitution have been studied on structural, electrical and morphological properties of BSCCO systems. Samples were prepared by a conventional solid-state reaction method with nominal composition $Bi_{1.65}Pb_{0.35-x}Nb_xSr_2Ca_2Cu_3O_{10+\delta}$ with $x = 0.0, 0.1, 0.2, 0.3, 0.35$. Structural and superconducting properties of all samples were investigated, and the relation between those was determined.

2 Experimental Procedures

The $Bi_{1.65}Pb_{0.35-x}Nb_xSr_2Ca_2Cu_3O_{10+\delta}$ (Bi, Pb)-2223 bulk samples were prepared from ultra-fine and high-grade purity powders of Bi_2O_3, PbO, $SrCO_3$, $CaCO_3$, Nb_2O_5 and CuO with purity of 99.99% using the conventional solid-state reaction method [20]. The starting powders were weighted and well mixed (the precursors were ground approximately for 1 h) in stoichiometric proportions. In order to remove any remaining volatile materials and initiate the formation of the superconducting phases, the prepared mixture was calcinated at 810 °C for 48 h. Then, samples were reground and mixed in an agate mortar pestle. The resulting powder from the first calcination process was pressed into disk-shaped pellets and sintered at 825 °C in air for 48 h. Finally, the pellets were sintered at 845 °C for 100 h and slowly furnace cooled down to room temperature. All of the calcination and sintering processes were performed using a programmable furnace. In calcination and sintering processes, samples were prepared under the pressures of 250 and 450 MPa, respectively. By using a hydraulic pressing machine, powder of the samples was converted into the disks with 13 mm diameter and 2 mm thickness. The samples are labeled as A ($x = 0.0$), B ($x = 0.1$), C ($x = 0.2$), D ($x = 0.3$) and E ($x = 0.35$).

The electrical resistivity of all the samples was measured as a function of temperature from 30 to 115 K using the standard four-probe method. The crystal structure of the samples was evaluated by SIEMENS X-ray diffractometer with CuK_α (1.54 Å) radiation. Lattice parameters of samples were obtained using Match 3.3 and FullProf_Suite_2014 softwares based on Cohen's least square method from the XRD patterns. Temperature- dependent magnetic characterizations of the samples were done by a vibrating sample magnetometer (Quantum Design). Scanning electron microscopy (SEM) images were taken by using BILKEN in order to investigate the microstructure of samples.

3 Results and Discussion

Figure 1 shows the XRD patterns of all samples after the final sintering process. All the peaks can be well indexed to Bi-2223(H) and Bi-2212 (L), as donated by Miller indices. The dominant phase in all of the samples is high-T_c (Bi-2223). Meanwhile, other phases such as Bi-2212 and impurity phases of $SrNbO_3$, $SrCu_2O_2$, $CuNb_2O_6$, $CaCuO_3$ and CuO peak were detected in the diffraction angle 2θ range between 2 and 60°. Similar results for CuO impurity were presented previously by other researchers [21,22]. Bilgili et al. showed that the volume fraction of high-Tc Bi-2223 phase decreased with increasing Nb addition up to $x = 0.20$. Results of this research agree with Bilgili et al., and moreover, substitution of Pb^{2+} ions with Nb^{5+} ions increases the impurity of samples. By increasing the niobium (with melting point = 1512 °C) substitution in the samples, this element is not dissolved completely within the main matrix during the heat treatment cycle. Niobium participates in the formation of the various impurity phases. In the sample, C niobium has solely participated in the formation of the $CuNb_2O_6$ impurity, but in samples D and E not only has participated in the formation of $CuNb_2O_6$ impurity but also in the formation of $SrNbO_3$ impurity. It can be seen

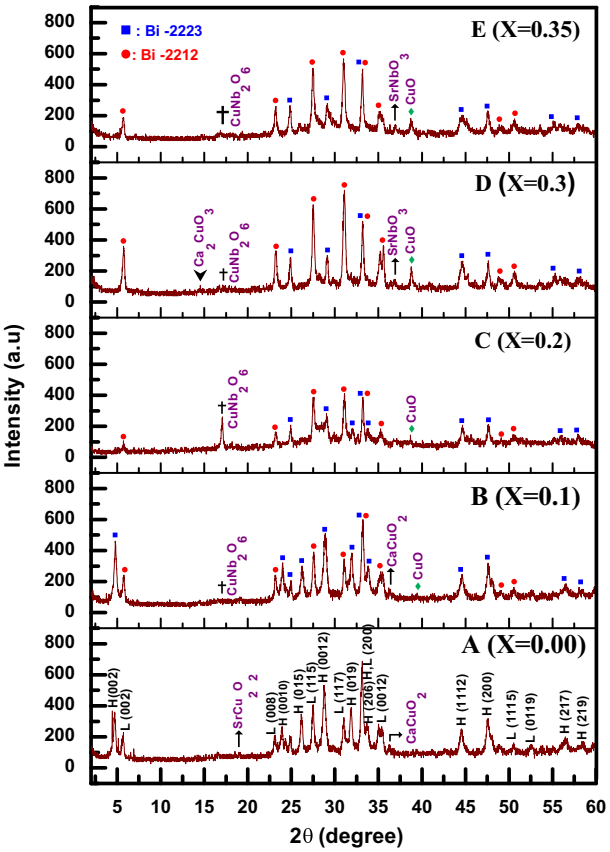

Fig. 1 XRD patterns of the samples *A*–*E* (Color figure online)

from the XRD patterns that the intensity of *H* (002) peak at $2\theta = 4.80°$ and *H* (206) peak at $2\theta = 33.98°$ first increases at $x = 0.1$, and then, they disappear. Similar to Celebi et al., the calculation of volume fraction of Bi-2223 and Bi-2212 phases was evaluated with the integrated intensity of all the peaks of Bi-2223 and Bi-2212 phases although few other researchers used the number of phases such as (002) and (115) or (0010) and (008) peaks of Bi-2223 and Bi-2212 phases [23,24]. The calculated volume fractions of the samples are listed in Table 1.

For determining the volume fraction of the present phases of the samples, the following equations were used by means of corresponding XRD peaks [25,26]:

$$\text{Bi-2223}(\%) \approx \frac{\Sigma I\,(\text{Bi-2223})}{Q} \times 100 \tag{1}$$

$$\text{Bi-2212}(\%) \approx \frac{\Sigma I\,(\text{Bi-2212})}{Q} \times 100 \tag{2}$$

$$\text{Impurity}(\%) \approx \frac{\Sigma I\,(\text{Impurity})}{Q} \times 100 \tag{3}$$

Table 1 Percentage volume fraction of formed phases in the samples

Sample	Bi-2223 (%)	Bi-2212 (%)	Impurity (%)
A ($x = 0.0$)	56.7	35.2	8.1
B ($x = 0.1$)	55.2	36.1	8.7
C ($x = 0.2$)	44.2	37.9	17.9
D ($x = 0.3$)	38.9	47.3	13.8
E ($x = 0.35$)	41.5	46.3	12.2

Table 2 Summary of critical temperature T_c^{offset}, T_c^{onset}, ΔT_c, p value and cell parameters of Bi-2223 phase for Nb substitution

Sample	T_c^{offset} (K)	T_c^{onset} (K)	ΔT_c (K)	a (Å)	b (Å)	c (Å)	p value
A ($x = 0.00$)	95.1	112.3	17.2	5.39441	5.38239	30.74105	0.119
B ($x = 0.1$)	80.4	102.3	21.9	5.39746	5.40539	30.71520	0.103
C ($x = 0.2$)	67.1	106.5	39.4	5.40428	5.39602	30.74809	0.091
D ($x = 0.3$)	51.7	79.4	27.7	5.40200	5.40112	30.69309	0.080
E ($x = 0.35$)	46.8	77.3	30.5	5.40588	5.40335	30.69016	0.076

where

$$Q = \Sigma I \text{ (Bi-2223)} + \Sigma I \text{ (Bi-2212)} + \Sigma I \text{ (Impurity)}$$

In the above equations, I is the intensity of present phases. As shown in Table 1, as the concentration of Nb is substituted with Pb increases up to 85%, high-T_c (Bi-2223) phase gradually decreases, while the low-T_c (Bi-2212) phase increases. However, if all of the Pb atoms were substituted with Nb, Bi-2223 phase slightly increases, while Bi-2212 phase decreases.

The unit cell parameters of the XRD peaks were calculated using Cohen's least squares method and using Match 3.3 and FullProf_Suite_2014 software which are listed in Table 2. The uncertainty of the crystal lattice parameter in this software remained in the ±0.00001 range. It is found that all of the samples have an orthorhombic structure similar to the results reported in the literature [27,28]. For the lattice parameters of $Bi_{1.65}Pb_{0.35-x}Nb_xSr_2Ca2Cu_3O_{10+\delta}$, a-axis except sample C increased from 5.39441 to 5.40588 Å, while c-axis except sample C decreased from 30.74105 to 30.69016 Å monotonically with increasing Nb substation (x) from 0.0 to 0.35. The reason for unexpected changes in a and c lattice parameters can be due to the existence of high impurity in this sample as indicated in Table 1. Also, the reason for to change in b lattice parameter in sample B can be due to an increase in the intensity of H (002) and H (206) peaks as indicated in Fig. 1. These monotonical changes of the lattice parameters not solely originate from a differing in atomic radius of (Nb^{+5} = 0.07 nm, Pb^{+2} = 0.119 nm), they could also be correlated with the decreasing hole concentration in the CuO_2 plane, as suggested by Satyavathi et al. [29] and Zandbergen et al.

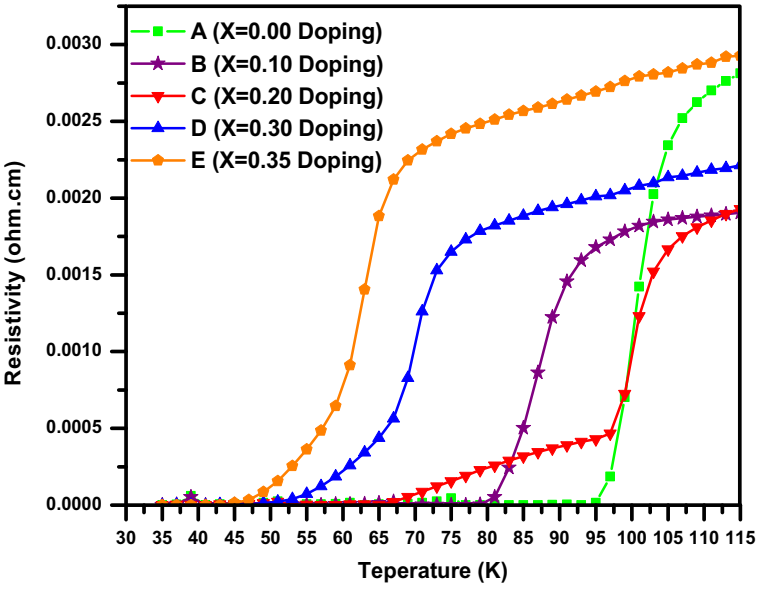

Fig. 2 Electrical resistivity versus temperature curves for samples (Color figure online)

[30]. The replacement of Nb^{+5} with Pb^{+2} may allow higher oxygen atoms to reside in the bismuth oxide layer, causing an extension along the a-axis and contraction along c-axis.

Figure 2 shows the temperature dependence of the electrical resistivity for all the $Bi_{1.65}Pb_{0.35-x}Nb_xSr_2Ca_2Cu_3O_{10+\delta}$ samples. Here onset critical temperature (T_c^{onset}) was defined as the temperature where resistance-temperature plot deviates from linearity and the resistance starts to decrease significantly, whereas the offset transition temperature (T_c^{offset}) was defined as the temperature at which $R = 0\ \Omega$. Metallic behavior is observed in all the samples above zero resistivity transition temperature. It is recognizable that the resistivity behavior obviously depends on the Nb concentration. The value of resistivity corresponding to $T = 115$ K of samples (A–E) is 0.00281, 0.00219, 0.00224, 0.00254 and 0.00377 Ω cm, respectively. Sample B with $x = 0.1$ Nb content has the lowest value of the resistivity. With substituting 0.1 Nb, resistivity decreases, but as it can be seen from results, there is almost regular increasing in the value of resistivity containing Nb content. Table 2 summarizes the value of T_c^{onset}, T_c^{offset} and transition width $\Delta T_c = T_c^{onset} - T_c^{offset}$ for all the samples. As can be seen, T_c^{offset} starts at the maximum of 95.1 K for sample A with no Nb, shifts to lower temperatures with increasing Nb content and reaches a minimum value of 46.8 K for sample E with $x = 0.35$. The reduction in critical temperature can be correlated with the reduced Bi-2223 phase as consistent with the XRD results. Similar Nb-content-dependent behavior of T_c^{offset} was observed for Nd- and Gd-substituted BSCCO system, in which T_c decreases with the increase Nd and Gd content, respectively [31,32]. Also, the ΔT_c value of the samples also increases as the Nb content increases with the exception of sample C. The reason for Sample C to disrupt the

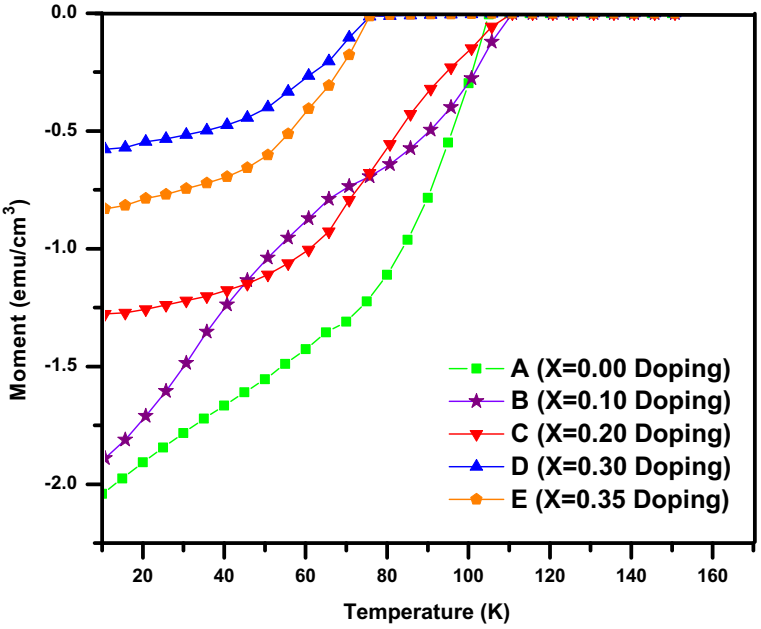

Fig. 3 Magnetization versus temperature curves for all samples with an applied field of 50 Oe (Color figure online)

variation in ΔT_c trend could be the presence of $CuNb_2O_6$ impurity phase. Also, the intergrowth of impurity phases, the weak coupling between the impurities and superconductor grains, and structural distortions may be revealed a decrease in the T_c^{onset} and T_c^{offset} values and decrease in ΔT_c.

The temperature dependencies of the zero-field-cooled (ZFC) magnetization of BSCCO samples measured under an external applied magnetic field of 50 Oe along the c-axis are indicated in Fig. 3. Below the onset temperature, all of the samples become diamagnetic. Superconducting BSCCO samples with lower Nb content have higher superconducting transition temperatures (T_c) than high Nb containing samples. As shown in Fig. 3, sample B ($x = 0.1$) shows the highest two-step decrease with temperature and deviates from the other samples. The reason for two-step reduction reflects from the flux shielding between and into the grains. The diamagnetic onset temperature was observed in the range of $T_c^{onset} = 77$–112 K which is depending on the amount of Nb substitution. The minimum critical temperature 77 K corresponds to the Pb-free sample. Substitution of a lead ion by an ion with a smaller diameter affects the lattice constant and critical temperature (T_c).

The DC hysteresis cycles are very useful in determining the intergranular critical current density in the superconductors. Therefore, the magnetic hysteresis cycles were measured at 10 K for all samples between the applied fields of ±9000 Oe and the results are shown in Fig. 4. The diamagnetic behavior observed in the M–H loops of all samples confirms the occurrence of conventional type II superconductivity. The overall features measured at $T = 10$ K are similar to each other in that the M-H loops display

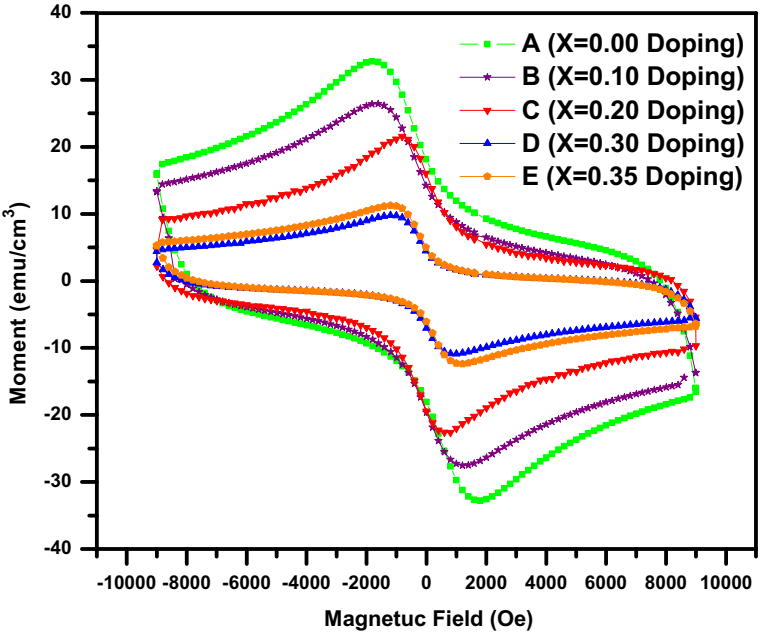

Fig. 4 M–H hysteresis curves for all samples at a temperature of 10 K (Color figure online)

an asymmetric profile in the field increasing and decreasing branches. Irreversible hysteretic magnetization is related to the delayed vortex penetration caused by the presence of a potential barrier of geometrical origin, as described by Bean's critical state model [33]. It can be seen from Fig. 4 that the penetration field and the magnitude of magnetization decrease with increasing Nb content. Sample *D* among the samples has the minimum closed hysteresis curve, due to the reduction in the Bi-2223 phase. For this reason, the superconducting properties of sample *D* are much worse than that of the others. The critical current density (J_c) of samples was evaluated from the hysteresis loops by using the Bean's critical state model [33]. In this model, the critical current density is proportional to the width of the hysteresis loop $\Delta M = |M_+ - M_-|$ and is given by this formula:

$$J_c = 20\frac{|\Delta M|}{b\left(1 - \frac{b}{3a}\right)} \tag{4}$$

In this formula, a and b ($a > b$) are the sample dimensions perpendicular to the applied field and ΔM is the difference between magnetization values recorded at the same field in the increasing and decreasing field branches. Critical current density (J_c) versus applied magnetic field curves are illustrated in Fig. 5. The highest critical current density values of samples are 4.60×10^3, 3.81×10^3, 3.28×10^3, 1.36×10^3 and 1.53×10^3 A cm^{-2} for the samples *A*, *B*, *C*, *D* and *E*, respectively. The sample *A* with no addition of Nb has the highest critical current density. In addition, the crit-

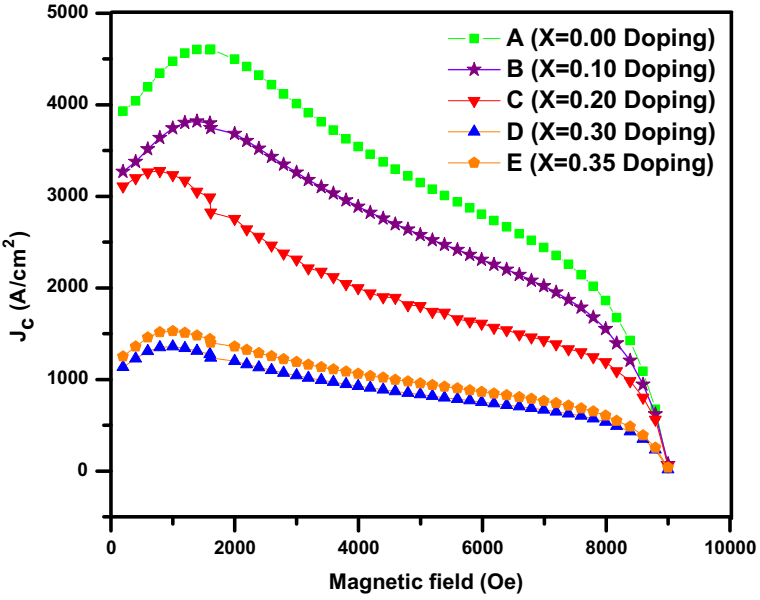

Fig. 5 Critical current density versus magnetic field of all samples (Color figure online)

ical current density of samples drop with increasing in Nb content up to $x = 0.3$; however, it increases with further increase in Nb content. In the high-T_c superconductors, J_c can be decreased by decreasing the volume fraction of the Bi-2223 phase and increasing the volume fraction of Bi-2212 phase. Also, non-superconducting impurity phases are effective in the flux-pinning mechanism. As shown in Table 1, the sample *D* has higher density of impurity phases than that of sample and highest Bi-2212 phase among the samples. Due to impurities, in the sample *D* the applied field begins to penetrate into the sample and decreases the critical current density value.

In ceramic high-temperature superconductors, one of the most important properties is their grain structure. These grain structures can be illustrated and explained by the SEM micrographs. These SEM micrographs provide us with data about the formation of the surface morphology of the samples. Surface morphology micrographs of the samples *A* and *E* taken by SEM and are shown in Fig. 6a, b. The microstructure of the samples consists of a common feature of grains which are randomly distributed. Similar grains are also obtained by other groups [34]. The grain size and the distribution of grains on the surfaces of the samples are quite different. The structure of sample *A* with no Nb^{+5} has platelike grains which is characteristic of the grain structure for Bi-2223 phase. In contrast, SEM micrograph of sample *E* with no Pb^{+2} contains the mixture of different sized flaky and platelike grains which are connected with each other, while there are some unfilled spaces among them as expected for the Bi-2212 phase. Consistent with XRD results, substitution of Nb^{+5} ions with Pb^{+2}, the Bi-2223 phase has gradually transformed into the Bi-2212.

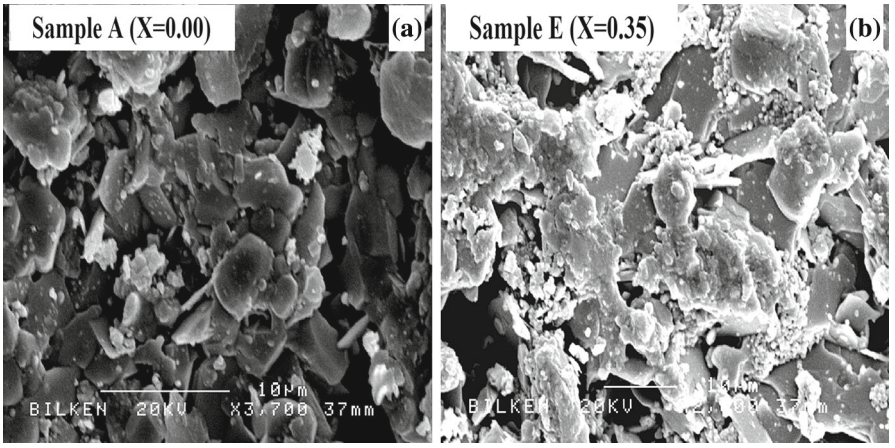

Fig. 6 **a–b** SEM micrographs for sample *A* and *E*

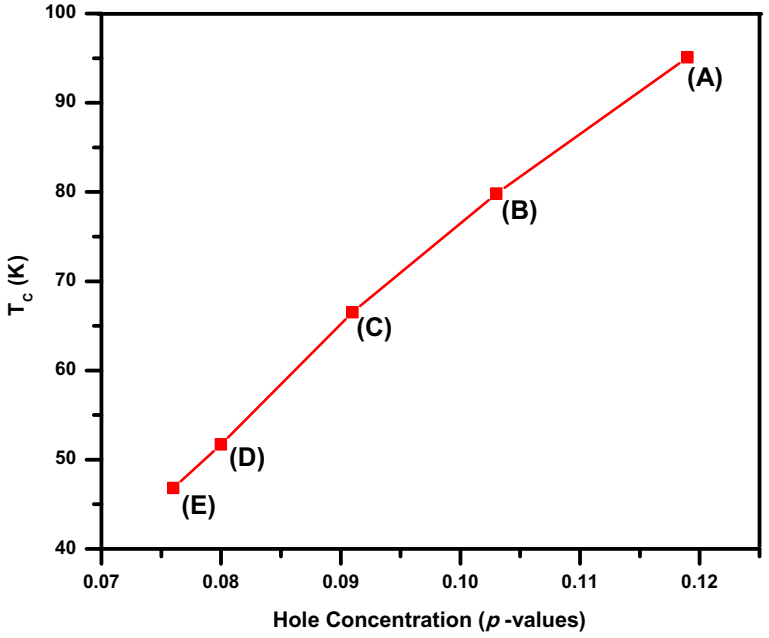

Fig. 7 Superconducting transition temperature versus p values of all samples (Color figure online)

The relationship between the superconducting transition temperature and the holes concentration p (the number of holes per Cu atom) is parabolic as shown in Fig. 7, and this relationship can be calculated using the formula which is given by Presland et al. [35].

$$\frac{T_c}{T_c^{max}} = 1 - 82.6\,(p - 0.16)^2 \tag{5}$$

In this formula, T_c^{max} is taken 110 K for the Bi-2223 system. Recently, this equation was successfully applied to Bi-based superconducting systems [36,37]. Earlier calculations for the unsubstituted Bi-2223 have shown that the values of p ranged from 0.116 to 0.160. In this study, p values calculated of the samples A to E are 0.119, 0.103, 0.091, 0.080 and 0.076, respectively. The monotonic decrease of hole concentration with increasing Nb content indicates that the increase in the normal-state resistivity value of the samples $\left(\rho \text{ at } T_c^{onset}\right)$ can be attributed to hole filling mechanism, as presented by Ekicibil et al. [38].

4 Conclusion

In this research, a systematic investigation of the influence of Nb substitution on the phase formation and superconducting properties of Bi-based superconductors have been performed. The high-T_c Bi-2223 phase in the BSCCO system decreases by increasing the Nb content. Under the same condition, Bi-2212 and impurity phases increase. Mainly, the impurity phases lead to a decrease in the critical temperature with the substitution of Pb with Nb. Magnetization measurements reveal that the critical current density decreases by increasing the Nb content. Based on these observations, it can be concluded that Pb substitution by Nb in Bi-based superconductors affected the superconducting properties, negatively. In other words, Nb substitution in BPSCCO system influenced the microstructure of the samples and degraded the intergrain connectivity and average crystallite size of Bi-2223 grains. These results are confirmed by SEM, resistivity measurements and magnetization hysteresis measurements.

Acknowledgements The authors would like to thank Bilkent University, Ankara, Turkey, for helping us the SEM micrographs. The authors would also like to express their thanks to Professor Ali Gerncer, Center of Excellence for Superconductivity Research, Ankara University, Turkey, for helpful discussions.

References

1. B. Ozcelik, H. Gundogmus, D. Yazıcı, J. Mater. Sci. Mater. Electron. **25**, 2456 (2014)
2. H. Gundogmus, B. Ozcelik, A. Sotelo, M.A. Madre, J. Mater. Sci. Mater. Electron. **24**, 2568 (2013)
3. H. Maeda, Y. Tanaka, M. Fukutomi, T. Asano, Jpn. J. Appl. Phys. **27**, L209 (1988)
4. L. Gao, J.C. Huang, L.R. Meng, H.P. Hor, J. Bechtold, Y.Y. Sun, W.C. Chu, Z.Z. Sheng, M.A. Herman, Nature **332**, 623 (1988)
5. W.C. Chu, J. Bechtold, L. Gao, H.P. Hor, J.C. Huang, L.R. Meng, Y.Y. Sun, Y.Q. Wang, Y.Y. Zue, Phys. Rev. Lett. **60**, 941 (1988)
6. L.J. Tallon, G.R. Buckley, W.P. Gilbert, R.M. Presland, M.W.I. Brown, E.M. Bowder, A.L. Christian, R. Gafull, Nature **333**, 153 (1988)
7. J. Jiang, J.J. Abell, Supercond. Sci. Technol. **11**, 705 (1998)
8. B. Chevalier, B. Lepine, A. Lalerzin, J. Darriet, J. Eournau, J.M. Tarascn, Mater. Sci. Eng. **B2**, 277 (1989)
9. A. Biju, R.P. Aloysius, U. Syamaprasad, Mater. Lett. **61**, 648–654 (2007)
10. R. Shabna, P.M. Sarun, S. Vinu, U. Syamaprasad, J. Alloy. Compd. **481**, 797–801 (2009)
11. A. Biju, R.G. Abhilash Kumar, R.P. Aloysius, U. Syamaprasad, Supercond. Sci. Technol. **19**, 854–859 (2006)
12. S.M. Khalil, Smart Mater. Struct. **14**, 804–810 (2005)
13. A. Sedky, J. Phys. Chem. Solid **70**, 483–488 (2009)
14. M. Fujiwara, M. Nagae, Y. Kusano, T. Fujii, J. Takada, Phys. C **274**, 317–322 (1996)

15. A. Coşkun, A. Ekicibil, B. Ozcelık, K. Kıymac, Chin. Phys. Lett. **21**(10), 2041 (2004)
16. M. Kappinnen, A. Fukuoka, J. Wang, S. Tanaka, M. Ikemachi, H. Yamauchi, Phys. C **208**, 130 (1988)
17. I.H. Gul, M.A. Rehman, M. Ali, A. Maqsood, Phys. C **432**, 71–80 (2005)
18. N. Gazanfari, A. Kilic, A. Gencer, H. Ozkan, Solid State Commun. **144**, 210–2077 (2011)
19. O. Bilgili, K. Kocabaş, J. Mater. Sci. Mater. Electron. **25**, 2889 (2014)
20. M. Ismail, R. Abd-Shukor, I. Hamadneh, S.A. Halim, J. Mater. Sci. **39**, 3517 (2004)
21. I. Karaca, S. Celebi, A. Varilci, A.I. Malik, Supercond. Sci. Technol. **16**, 100–104 (2003)
22. P.V. Reddy, K. Ganesh, R.J. Topare, N.K. Sahuji, S.S. Shah, Phys. C Supercond. **253**, 89–96 (1995)
23. S.A. Saleh, Phys. C Supercond. **444**, 40–44 (2006)
24. G. Ilonca, A.V. Pop, T.R. Yang, I. Gr, C. Deac, R.Stiufiuc Lung, G. Stiufiuc, Int. J. Inorg. Mater. **3**, 769–772 (2001)
25. C.W. Chiu, R.L. Meng, L. Gao, Z.J. Huang, F. Chen, Y.Y. Xue, Nature **365**, 323 (1993)
26. I.V. Driessche, A. Buekenhoudt, K. Konstantinov, E. Brueneel, S. Hoste, Appl. Supercond. **4**, 185 (1996)
27. N. Turk, H. Gundogmus, M. Akyol, Z.D. Yakıncı, A. Ekicibil, B. Ozcelik, J. Supercond. Nov. Magn. **27**, 711–716 (2014)
28. B. Ozcelik, M. Gursul, A. Sotelo, M.A. Madre, J. Mater. Sci. Mater. Electron. **26**, 441–447 (2015)
29. S. Satyavathi, K.N. Kishore, V.H. Babu, O. Pena, Supercond. Sci. Technol. **9**, 93 (1996)
30. H.W. Zandbergen, W.A. Groen, A. Smit, G. Van Tendeloo, Phys. C **168**, 426 (1990)
31. B. Ozkurt, A. Ekicibil, M.A. Aksan, B. Ozcelik, M.E. Yakinci, K. Kiymac, J. Low Temp. Phys. **149**, 105–118 (2007)
32. A. Ekicibil, A. Coskun, B. Ozcelik, K. Kiymac, J. Low Temp. Phys. **140**, 105–117 (2005)
33. C.P. Bean, Rev. Mod. Phys. **36**, 31 (1964)
34. M. Takano, J. Takada, K. Oda, H. Kitaguchi, Y. Miura, Y. Ikeda, Y. Tomii, H. Mazaki, Jpn. J. Appl. Phys. **27**, L1041–L1043 (1988)
35. M.R. Presland, J.L. Tallon, R.G. Buckley, R.S. Liu, N.E. Floer, Phys. C **176**, 95 (1991)
36. S.D. Obertelli, J.R. Cooper, J.L. Tallon, Phys. Rev. B **46**, 14928 (1992)
37. D.R. Sita, R. Singh, Phys. C **296**, 21 (1998)
38. H. Gondogmus, M. Akyol, Z.D. Yakinci, A. Ekicibil, J. Supercond. Nov. Magn. **27**, 711–716 (2014)